Supplementary Information

Synergistic promotion of the oxygen evolution reaction by Co and Fe dual-doping of NiS_2

Wen-juan Xu, Ying-yu Wang, Jiang-yan Dang, Xiao-ying Zhang*, Wen-liang Li*, Jing-ping Zhang*

Faculty of Chemistry, Northeast Normal University, Changchun 130024, P. R. China.

* Corresponding authors

Email addresses: zhangxy218@nenu.edu.cn (X.-Y. Zhang); liwl926@nenu.edu.cn (W.-L. Li); jpzhang@nenu.edu.cn (J.-P. Zhang)

1. Experimental section

1.1. Synthesis of NiS_2 on Ni foam

1 mmol $Ni(NO_3)_2 \cdot 6H_2O$, 2.5 mmol urea, and 1.8 mmol ammonium fluoride were dispersed into 70 ml of deionized water. The pretreated NF was immersed into the above solution subsequently transferred to a 100 ml Teflon-lined stainless-steel autoclave and kept at 90°C for 10 hours. It was naturally cooled to room temperature, washed with deionized water to remove the residue and vacuum dried to obtain Ni-pre. The obtained Ni-pre was immersed into a 70 ml solution containing 1.5 mmol $Na_2S \cdot 9H_2O$ and subsequently transferred to a 100 ml Teflon-lined stainless steel autoclave and kept in a hydrothermal reaction at 90°C for 10 hours. It was naturally cooled to room temperature, washed with deionized water to remove the residue and vacuum dried to obtain NiS_2.

1.2. Synthesis of Fe-NiS_2 on Ni foam

1 mmol $Ni(NO_3)_2 \cdot 6H_2O$, 1 mmol $Fe(NO_3)_3 \cdot 9H_2O$, 2.5 mmol urea, and 1.8 mmol ammonium fluoride were dispersed into 70 ml of deionized water. The pretreated NF was immersed into the above solution subsequently transferred to a 100 ml Teflon-lined stainless-steel autoclave and kept at 90°C for 10 hours. It was naturally cooled to room temperature, washed with deionized water to remove the residue and vacuum dried to obtain Fe-Ni-pre. The obtained Fe-Ni-pre was immersed into a 70 ml solution containing 1.5 mmol $Na_2S \cdot 9H_2O$ and subsequently transferred to a 100 ml Teflon-lined stainless steel autoclave and kept in a hydrothermal reaction at 90°C for 10 hours. It was naturally cooled to room temperature, washed with deionized water to remove the residue and vacuum dried to obtain Fe-NiS_2.

1.3. Synthesis of Co-NiS_2 on Ni foam

In a similar manner as the Fe-NiS_2 synthesis method described above, Co-NiS_2 was prepared except that the $Fe(NO_3)_3 \cdot 9H_2O$ is substituted with $Co(NO_3)_2 \cdot 6H_2O$.

1.4. Characterizations

The x-ray powder diffraction measurements with a Smartlab diffractometer in the range of 10°~80° (Cu target Kα, λ = 1.5418 Å). The surface morphology of the samples was observed by field emission scanning electron microscopy (Hitachi SU-8000 FE-SEM), and the composition of the samples was analyzed by energy dispersive x-ray energy spectrometry (EDS). The chemical states and elemental compositions of the samples were determined by X-ray photoelectron spectroscopy (XPS, USWHA150) under monochromatic Al-Kα irradiation. Transmission electron microscopy (TEM), HRTEM images and selected area electron diffraction (SAED) of the samples were obtained by transmission electron

microscopy (JEOL-2100F). The BET specific surface area and pore size distribution of the samples were determined by nitrogen adsorption/desorption BELSORP max apparatus (Particle Sciences, USA). Atomic ratios were determined by atomic absorption spectroscopy (AAS).

1.5. Electrochemical measurements

All electrochemical tests were performed at the CHI760E electrochemical workstation, using a classic three-electrode cell. At room temperature, the Hg/HgO electrode was used as the reference electrode, the platinum wire was used as the counter electrode, and the Ni foam based electrocatalyst was directly used as the working electrode. The electrolyte for all tests was the 1 M KOH solution (pH 13.8). All the potentials herein were converted to the reversible hydrogen electrode (RHE) by the following equation: $E_{(RHE)} = E_{(vs\cdot Hg/HgO)} + 0.0592 \times pH + 0.098$. The linear scan voltammetry (LSV) curves were measured at a scan rate of 5 mV s^{-1} with 95% iR compensation. The Tafel slope was obtained from the corresponding LSV curve by plotting the overpotential logarithmic current density (*j*). The double layer capacitance (C_{dl}) was obtained by cyclic voltammetry (CV) curves in the non-Faraday region of 0.67-0.77 V *vs*. RHE at different scan rates (20, 40, 60, 80 and 100 mV s^{-1}). The electrochemically active surface area (ESCA) was then calculated via equation: ECSA = C_{dl}/C_S. where Cs is specific capacitance of electrocatalysts (0.04 mF cm^{-2}). Electrochemical impedance spectroscopy (EIS) was conducted at a potential of 1.524 V *vs*. RHE over the frequency range from 100000 to 0.01 Hz at an amplitude of 5 mV. Durability was tested in the KOH electrolyte with a constant current of 700 mA cm^{-2} using the chronoamperometry (CP) technology (without iR compensation). The Faraday efficiency is tested at 0.1 A and

calculated by the formula FE% = 4nF/It ×100%, where 4 is the number of electrons transferred by the OER, n is the number of moles of gas generated, F is the Faraday constant (96,485C mol^{-1}), I is the current and t is the time.

1.6. Theoretical calculation

In this study, using the computational hydrogen electrode model proposed by Nørskov and co-workers, the Gibbs free energy change (ΔG) of each OER elementary step was calculated via equation 1 [1]：

$$\Delta G = \Delta E + \Delta ZPE - T\Delta S + \Delta G_U + \Delta G_{pH} \quad (1)$$

where ΔE represents the reaction energy change, which is directly obtained by DFT calculations. ΔZPE, T, and ΔS indicate difference in zero-point energy, the temperature (298.15 K), and the entropy difference, respectively. The zero point energies and entropy of gas-phase molecules (H_2 and H_2O) were obtained from the thermodynamic NIST database, while those of the oxygenated adsorbates were calculated from the vibrational frequencies by quasi-harmonic approximation. ΔG_U and ΔG_{pH} are the electrode potential and the free energy changes caused by variations inthe H^+ concentrations, respectively.

At alkaline environment, the overall OER process includes four steps [2]:

$$* + OH^- \rightarrow *OH + e^- \quad (2)$$

$$*OH + OH^- \rightarrow *O + H_2O + e^- \quad (3)$$

$$*O + OH^- \rightarrow *OOH + e^- \quad (4)$$

$$*OOH + OH^- \rightarrow O_2 + H_2O + e^- + * \quad (5)$$

where * represents an adsorption site on the catalyst, and *OH, *O, and *OOH denote the corresponding absorbed intermediates. At standard conditions, the Gibbs free energy changes

for each step (ΔG_{1-4}) can be expressed as:

$$\Delta G_1 = E_{(*OH)} - E_{(*)} - E_{H_2O} + 1/2E_{H_2} + (\Delta ZPE - T\Delta S)_1 - eU \quad (6)$$

$$\Delta G_2 = E_{(*O)} - E_{(*OH)} + 1/2E_{H_2} + (\Delta ZPE - T\Delta S)_2 - eU \quad (7)$$

$$\Delta G_3 = E_{(*OOH)} - E_{(*O)} - E_{H_2O} + 1/2E_{H_2} + (\Delta ZPE - T\Delta S)_3 - eU \quad (8)$$

$$\Delta G_4 = E_{(*)} - E_{(*OOH)} + E_{O_2} + 1/2E_{H_2} + (\Delta ZPE - T\Delta S)_4 - eU \quad (9)$$

Here, $E_{(*)}$, $E_{(*OH)}$, $E_{(*O)}$ and $E_{(*OOH)}$ can be obtained by the calculated DFT total energy of the pristine substrate and those absorbed with OH, O, and OOH, respectively. E_{H_2O} and E_{H_2} are the total energy of H_2O and H_2 molecules in the gas phase, respectively.

2. Results and discussion

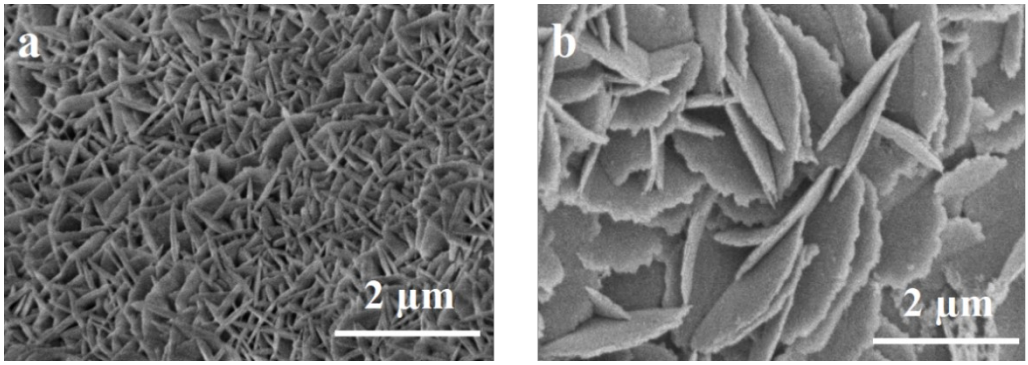

Fig. S1. SEM images of (a) Co,Fe-Ni Precursor and (b) NiS_2.

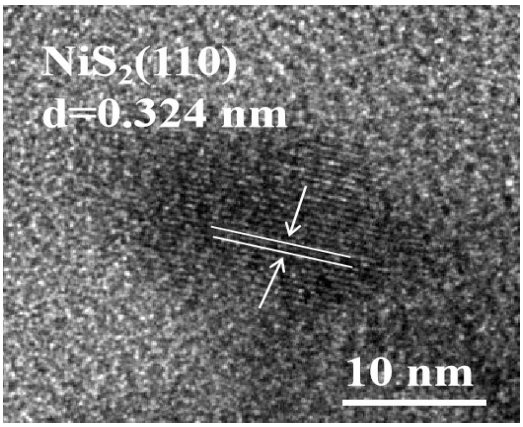

Fig. S2. HRTEM image of NiS_2.

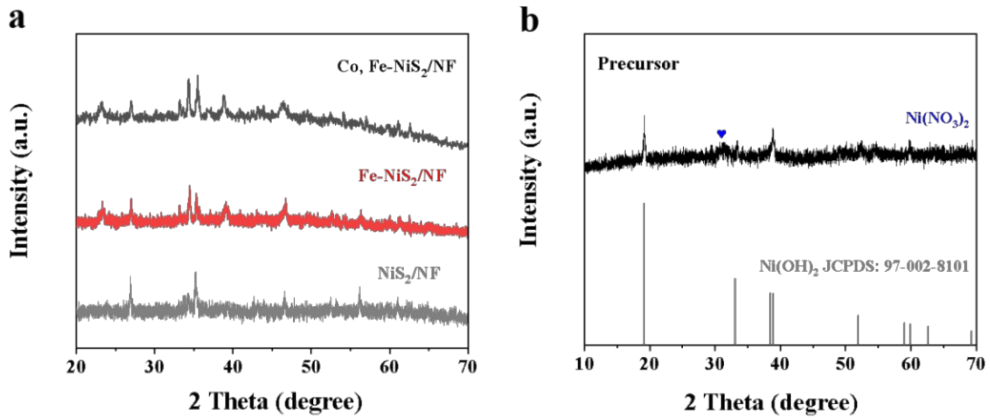

Fig. S3. XRD patterns of (a) NiS_2, Fe-NiS_2 and (b) Co,Fe-Ni Precursor.

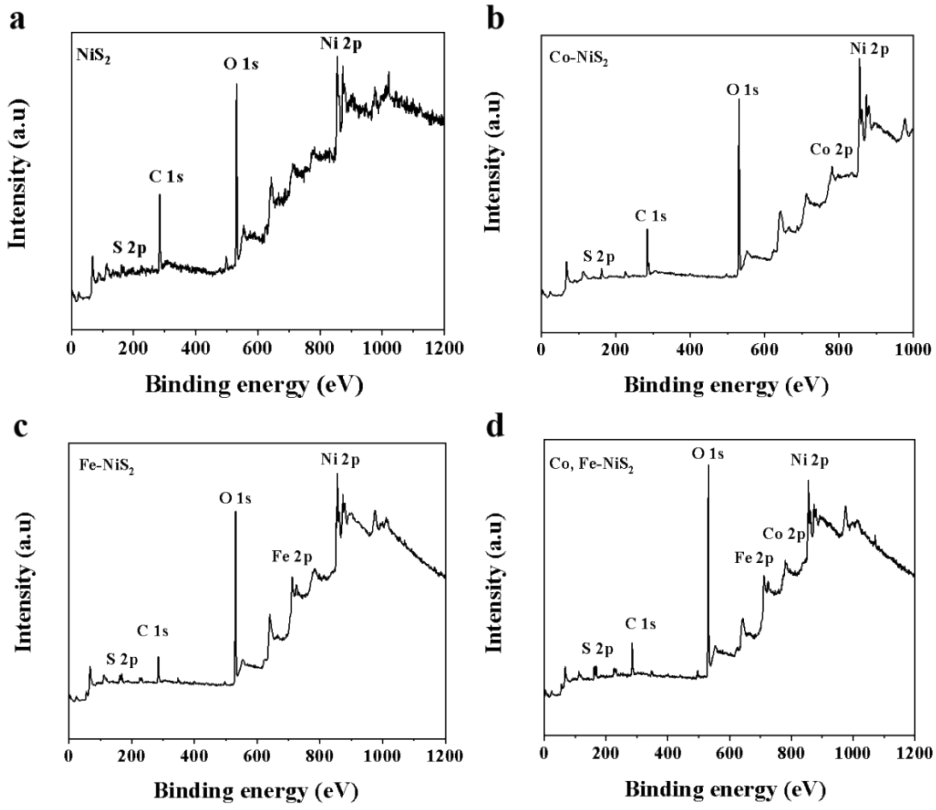

Fig. S4. The XPS survey spectra of (a) NiS_2, (b) Co-NiS_2, (c) Fe-NiS_2 and (d) **Co,Fe-NiS_2**.

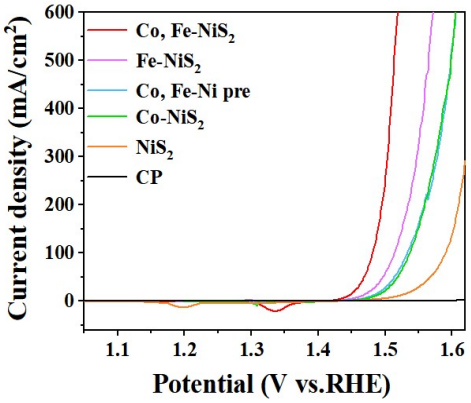

Fig. S5. OER polarisation curves in 1.0 M KOH based on carbon paper as substrate.

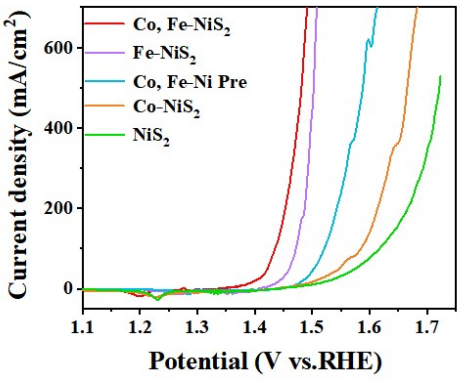

Fig. S6. Negative sweep OER polarization curves in 1.0 M KOH of catalysts.

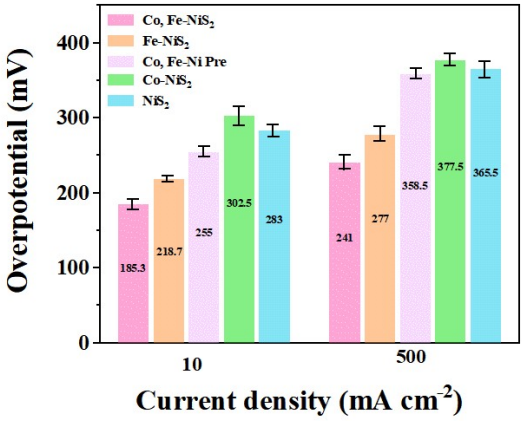

Fig. S7. Overpotential obtained in repeated experiments. Error bars refer to the standard

deviations for at least three independent tests.

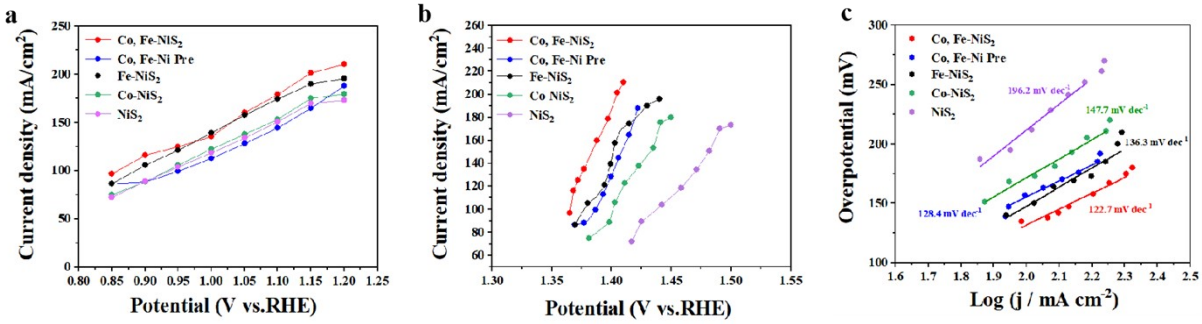

Fig. S8. (a) Sampled OER current-voltage plot, (b) 100% iR drop-corrected current-voltage plot, (c) Steady-state polarisation curve constructed from OER currents (Tafel plot).

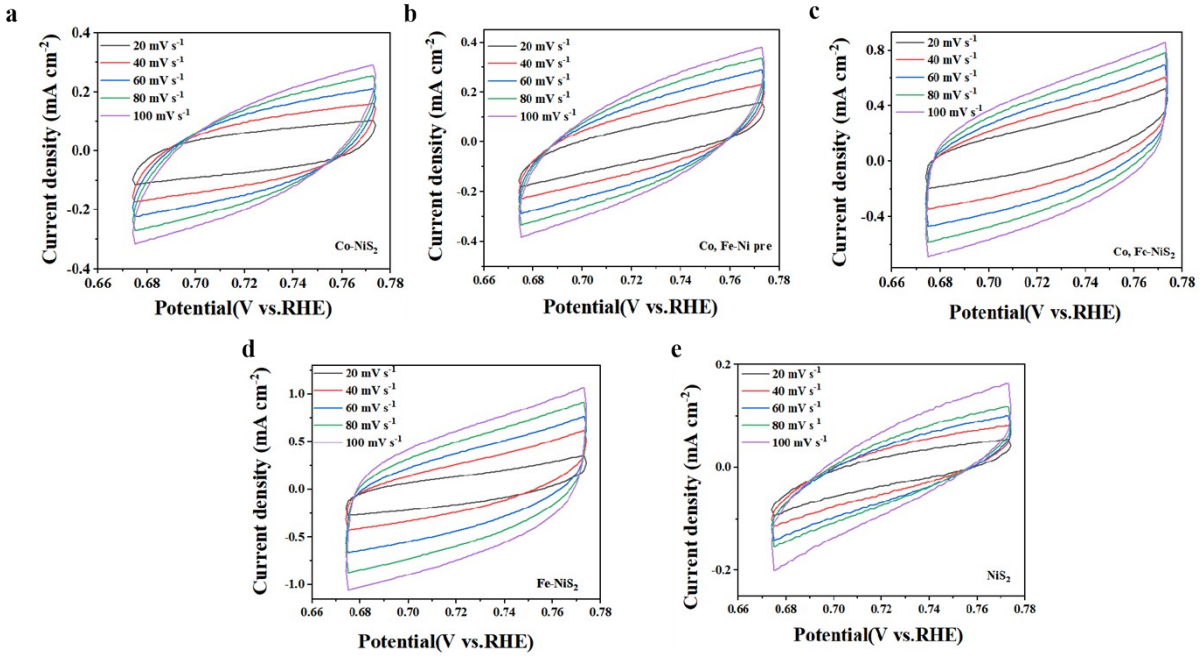

Fig. S9. CV curves of (a) NiS_2, (b) Co-NiS_2, (c) Fe-NiS_2, (d) Co,Fe-Ni pre and (e) **Co,Fe-NiS_2** recorded in the region of 0.83-0.93 V *vs*. RHE for OER in 1 M KOH.

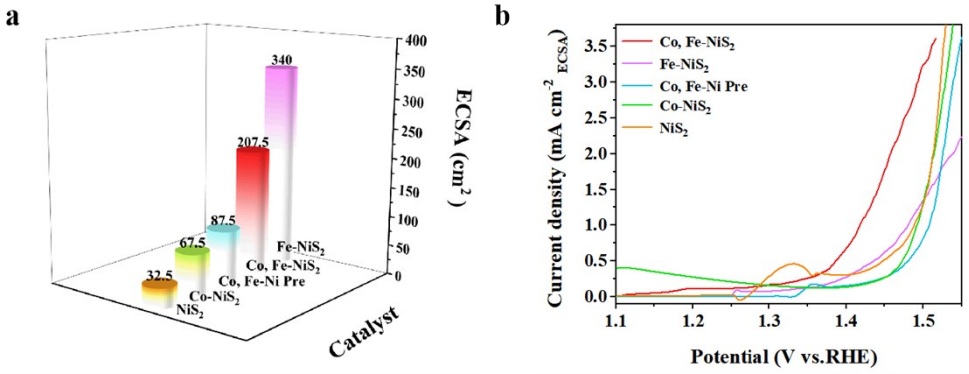

Fig. S10. (a) The ECSA of catalysts in the non-faradaic region, (b) Polarization curves normalized by the ECSA of **Co,Fe-NiS$_2$** and its contrast samples in OER.

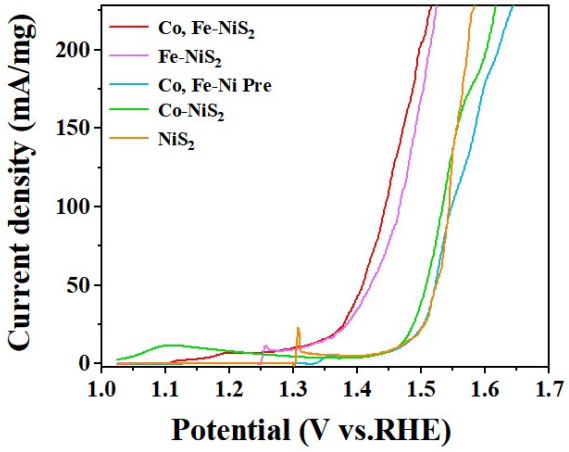

Fig. S11. Mass-normalised LSV Curve in 1.0 M KOH.

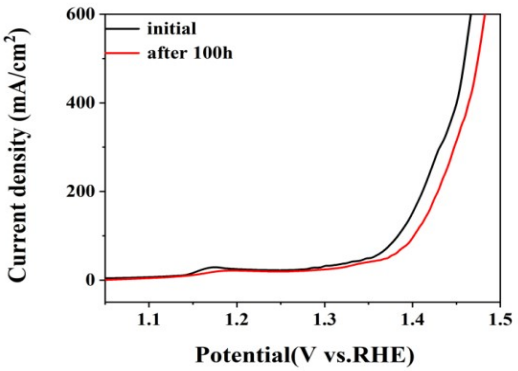

Fig. S12. OER polarization curves for **Co,Fe-NiS$_2$** before and after 100 h stability tests.

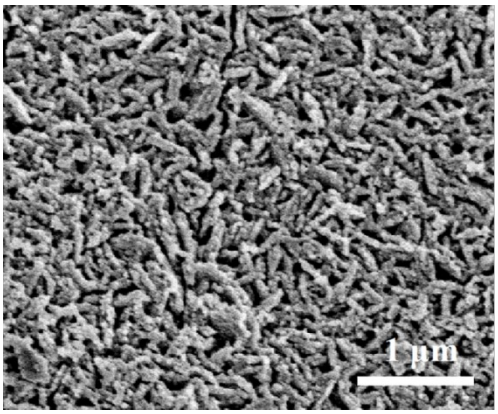

Fig. S13. SEM images of **Co,Fe-NiS_2** after 100 h stability test.

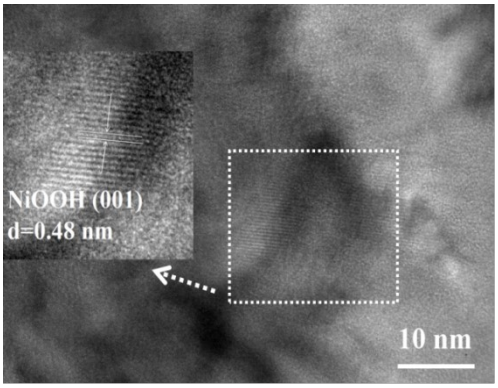

Fig. S14. HRTEM image of **Co,Fe-NiS_2** after OER stability.

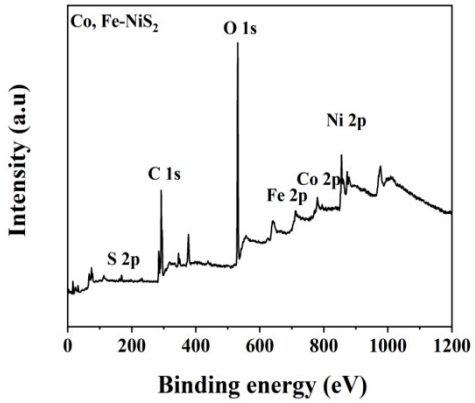

Fig. S15. The XPS survey spectra of **Co,Fe-NiS_2** after 100 h stability test.

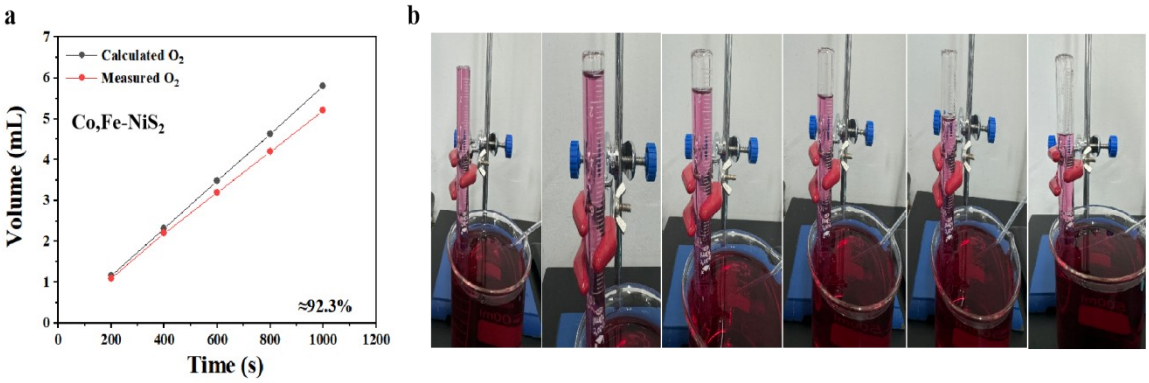

Fig. S16. (a) The gas volume changes with time (interval 200 seconds), (b) Photographs of the gas produced by the anode at different times.

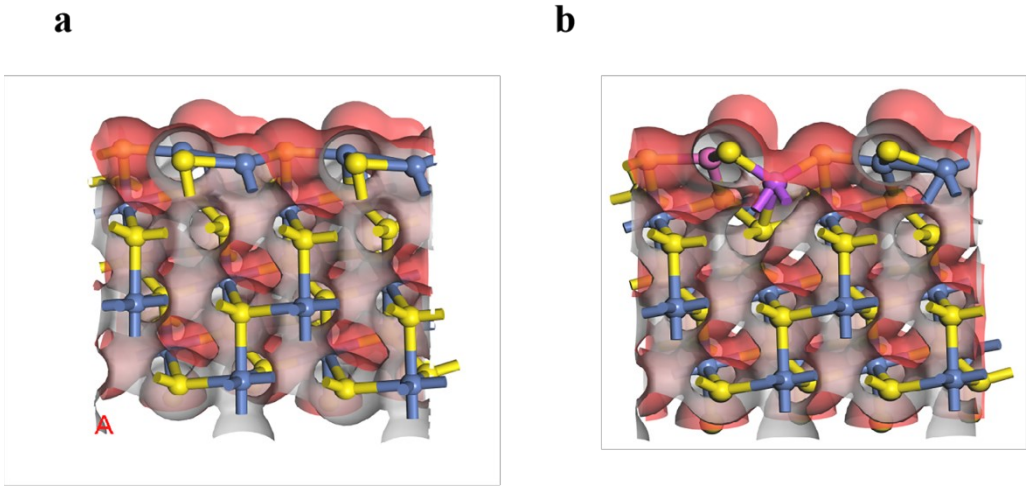

Fig. S17. Charge density diagram of (a) NiS_2 and (b) **Co,Fe-NiS_2**.

Table S1. Elemental ratios for **Co,Fe-NiS_2**.

Catalysts	Fe(wt.%)	Co(wt.%)	Ni(wt.%)	S(wt.%)
Co,Fe-NiS_2	**5.4**	**6.1**	**21.3**	**67.2**

Table S2. R_S and Rct of samples for IR compensation.

Catalysts	RS (Ω)	Rct (Ω)
Co,Fe-NiS_2	3.25	2.09
Fe-NiS_2	4.03	2.51
Co,Fe-Ni pre	3.39	25.73
Co-NiS_2	3.66	2.91
NiS_2	3.46	6.72

Table S3. Catalyst mass loading.

Catalysts	**Mass loading(mg cm^{-2})**
Co,Fe-NiS_2	3.3
Fe-NiS_2	2.7
Co-NiS_2	2.3
NiS_2	2.2
Co,Fe-Ni pre	3.1

Table S4. Mulliken atomic charges.

NiS_2	**Co,Fe-NiS_2**

atomic	charge	atomic	charge
Ni (1)	0.276	Ni (1)	0.285
Ni (2)	0.308	Ni (2)	0.31
Ni (3)	0.295	Ni (3)	0.306
Ni (4)	0.307	Ni (4)	0.315
S (5)	-0.047	S (5)	-0.049
S (6)	-0.136	S (6)	-0.147
S (7)	-0.122	S (7)	-0.12
S (8)	-0.153	S (8)	-0.162
S (9)	-0.048	S (9)	-0.051
S (10)	-0.154	S (10)	-0.212
S (11)	-0.115	S (11)	-0.12
S (12)	-0.139	S (12)	-0.143
Ni (13)	0.293	Ni (13)	0.31
Ni (14)	0.359	Ni (14)	0.332
Ni (15)	0.276	Ni (15)	0.286
Ni (16)	0.302	Ni (16)	0.304
S (17)	-0.139	S (17)	-0.146
S (18)	-0.351	S (18)	-0.342
S (19)	-0.117	S (19)	-0.121
S (20)	-0.159	S (20)	-0.191
S (21)	-0.138	S (21)	-0.15

S (22)	-0.33	S (22)	-0.25
S (23)	-0.122	S (23)	-0.121
S (24)	-0.147	S (24)	-0.178
Ni (25)	0.293	Ni (25)	0.301
Ni (26)	0.359	Co(26)	0.226
Ni (27)	0.276	Ni (27)	0.286
Ni (28)	0.302	Ni (28)	0.311
S (29)	-0.139	S (29)	-0.142
S (30)	-0.351	S (30)	-0.255
S (31)	-0.117	S (31)	-0.124
S (32)	-0.159	S (32)	-0.153
S (33)	-0.138	S (33)	-0.142
S (34)	-0.33	S (34)	-0.275
S (35)	-0.122	S (35)	-0.121
S (36)	-0.147	S (36)	-0.154
Ni (37)	0.276	Ni (37)	0.286
Ni (38)	0.308	Ni (38)	0.321
Ni (39)	0.295	Ni (39)	0.31
Ni (40)	0.307	Fe (40)	0.353
S (41)	-0.047	S (41)	-0.051
S (42)	-0.136	S (42)	-0.157
S (43)	-0.122	S (43)	-0.12

S (44)	-0.153	S (44)	-0.157
S (45)	-0.048	S (45)	-0.049
S (46)	-0.154	S (46)	-0.15
S (47)	-0.115	S (47)	-0.123
S (48)	-0.139	S (48)	-0.167

References

[1] Nørskov, J. K.; Rossmeisl, J.; Logadottir, A.; Lindqvist, L.; Kitchin, J. R.; Bligaard, T.; Jonsson, H. Origin of the Overpotential for Oxygen Reduction at a Fuel-Cell Cathode, J. Phys. Chem., B., 2004, 108, 17886-17892.

[2] Y.-Y. Wang, M. Qiao, Y.-F. Li, S.-Y. Wang, Tuning surface electronic configuration of NiFe LDHs nanosheets by introducing cation vacancies (Fe or Ni) as highly efficient electrocatalysts for oxygen evolution reaction, Small., 2018, 14, 1800136.